Applied Surface Science 718 (2026) 164918

Contents lists available at ScienceDirect

Applied Surface Science

journal homepage: www.elsevier.com/locate/apsusc

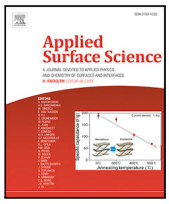

Full length article

Interaction of Li, Na and K overlayers with Pt(111): Structure and fundamental properties

Andrey A. Koverga [a,b,*], Edson A. Ticianelli [b], Axel Groß [a]

[a] Institute of Theoretical Chemistry, Ulm University, Ulm, Germany
[b] Instituto de Quimica de Sao Carlos, Universidade de Sao Paulo, Sao Carlos, SP, Brazil

ARTICLE INFO

Keywords:
DFT
Pt
Catalysis
Adatoms

ABSTRACT

In this computational study, the adsorption of alkali metal atoms on Pt(111) is studied by periodic electronic structure calculations based on density functional theory. This study is motivated by the promoting role of alkali metal atoms in several reactions in electro- and heterogeneous catalysis. In a systematic approach, we first study the explicit interaction of the atoms with the Pt(111) surface focusing on structural and electronic details of the alkali interaction with the metal substrate, also as a function of the adsorbate coverage. Furthermore, we contrast our findings with corresponding results for the anionic counterpart, the adsorption of halogen atoms, identifying common and diverse trends.

1. Introduction

The interaction of alkali metal (AM) atoms with metal surfaces is of strong current interest, in particular in the field of electrochemistry and electrocatalysis [1,2]. It is well-known that at electrochemical interfaces of metal electrodes AM cations typically adsorb non-specifically [3], i.e., with their solvation shell still intact, whereas for example halide anions adsorb specifically [4,5], i.e. in a chemisorption fashion. Still, in spite of the non-specific adsorption, it is known that the presence of alkali metal cations in the electrolyte can strongly affect important electrochemical processes taking place on metal catalysts such as the reduction of CO_2 [6–8], and oxygen [9,10], hydrogen evolution [11], and the electrooxidation of ethanol [12] and alcohols [13]. Interestingly, AM can act as promoter of a given reaction on some metallic catalysts and has no effect on another ones [10,13]. Outside of the electrochemical environment, alkali metals are often used as promoters in heterogeneous catalysis, for example for the ammonia synthesis on iron [14], the hydrogenation of alkynes and alkenes [15], and the CO and CO_2 hydrogenation [16–21].

The reasons behind the observed enhancement in the catalytic activity of the systems with the AM promoters has remained largely unresolved. In case of the electrochemical CO_2 reduction reaction it was suggested that hydrated alkali metal cations create a dipole field that has a stabilizing effect on the adsorption of CO_2 reduction intermediates with significant dipole moments, simultaneously decreasing CO_2 adsorption energy [6]. Other theories explain the AM-promoted CO_2 reduction reaction in terms of their effect on the interfacial electric field [7] and highlight the impact of alkali metal cations on the interaction of the CO with interfacial water, which is critical for ethylene formation [22]. In a similar fashion, the interfacial water structure and its destabilization induced by the alkali metal presence has been proposed as an important factor of enhanced oxygen reduction in alkaline solution [10]. It was also suggested, based on DFT simulations [1,23] that the reduction of CO_2 is promoted by the presence of partially desolvated metal cations that stabilize the CO_2 intermediate via short-range electrostatic interactions.

As for the hydrogen evolution reaction, it has been shown that the presence of small cations such as Li^+ induces a higher OH coverage on Pt, which promotes water dissociation and the Volmer step kinetics, leading to an improved overall activity [11] of this otherwise sluggish process in alkaline media. Outside of the electrochemical environment the ability of potassium to increase the bonding energy of nitrogen and reduce the activation energy of N_2 dissociation was tied to the improved ammonia synthesis rate on the iron catalyst [14]. Similarly, the enhanced CO dissociation on transition metal surfaces was attributed to the potassium-promoted strengthening of CO bonding [16].

Thus, despite the plethora of accumulated evidence demonstrating the promoting properties of alkali metals on the catalytic activity of other metals, the question of the fundamental basis of this enhancement remains largely under dispute. At the same time, it is a well-known fact that decorating metal surfaces with foreign atoms, or adatoms, affects their fundamental and catalytic properties [24–31]. In particular the modification of platinum – one of the best known single-element

* Corresponding author at: Institute of Theoretical Chemistry, Ulm University, Ulm, Germany.
E-mail address: akoverga@unal.edu.co (A.A. Koverga).

https://doi.org/10.1016/j.apsusc.2025.164918
Received 14 July 2025; Received in revised form 26 September 2025; Accepted 15 October 2025
Available online 24 October 2025

catalyst – with adatoms of other elements has drawn significant attention over the last several decades [32–42]. While there are reports on experimental studies of the high coverages of AM adatoms on Pt surfaces [18,43–45], the available fundamental-level works focus only on rather low Na and K adatom coverages, up to 0.25 ML [46,47]. Also, no information is available on coadsorption of several lithium atoms on platinum. Since it is an established fact that these systems demonstrate a significant variation of fundamental properties with coverage [43], the theoretical investigation of higher AM coverages on platinum is highly warranted.

In this regard, a study of Li, Na and K adlayers on platinum with two-dimensional geometry could provide important informations on the adsorption and interaction of AM atoms with other atoms in the adlayer and with the substrate. By considering only overlayers with a planar structure the study would be able to focus on the situation where all adsorbed atoms are able to interact with the substrate and that any adatom–adatom interaction is lateral, which is not possible upon formation of three-dimensional structures. It can also shed light on the factors driving growth and formation of AM structures on other metals [48]. The Pt(111) surface presents an attractive choice as a possible substrate, since it is densely packed and has not been reported to reconstruct at high AM coverages.

The present work aims to explore, by means of density functional theory calculations, the evolution of fundamental properties of alkali metals on Pt(111) in the coverage range where the AM overlayer retains its two-dimensional structure. We determine and discuss in detail the stability of the adsorbed atoms on the surface, the geometrical structure of the adlayer, the global work function of the composite systems and the adatom-induced charge redistribution in the surface. In addition, we consider a possible alkali metal incorporation into subsurfaces layers as well. We are confident that the findings of this work will be of interest in the fields of heterogeneous catalysis, electrocatalysis and material science in general.

2. Computational details

Spin-polarized periodic density functional calculations were carried out using the Vienna *ab initio* simulation package (VASP) code (version 6.4.2) [49–52]. The exchange–correlation energy was calculated using the generalized gradient approximation (GGA) by Perdew, Burke and Ernzerhof [53], which is a popular choice for studying transition-metal based systems and their fundamental characteristics [54–57]. The atomic cores were described with the Projector Augmented Wave (PAW) method [58], as implemented by Kresse and Joubert [59], with the following valence configurations: Pt – $5d^9 6s^1$, Li – $2s^1$, Na – $3s^1$, and K – $4s^1$. The electronic wave functions were expanded in a plane wave basis set with the energy cut-off set to 400 eV.

The platinum (111) surface was modeled as a 6-layer (4×4) supercell system created from the bulk structure with a calculated optimized lattice constant of 3.97 Å. For the specific alkali metal coverage of 0.33 ML reported in some experimental studies [18,46,47], a $(2\sqrt{3}\times 2\sqrt{3})$ cell was used. All calculations were carried out with a vacuum region of 18 Å preventing the interaction between the repeated cell images in z direction. In addition, a dipole correction scheme was applied in all cases to ensure that the slabs were decoupled. For the geometry optimization, the first irreducible Brillouin zone was sampled by 4 × 4 × 1 Monkhorst–Pack [60] k-points mesh while a denser 13 × 13 × 1 scheme was used for the density of states (DOS) calculations. In all cases the first order Methfessel–Paxton approach [61] was applied with a Gaussian width of smearing of 0.2 eV.

For the structure optimization, the three uppermost out of six total metal layers were allowed to relax, while the three bottom layers were frozen in the bulk-like geometry. The atoms present on the surfaces were allowed to relax in all three directions together with the upper three layers of platinum, the structural optimization was performed until the forces acting on all atoms were below 0.01 eV/Å.

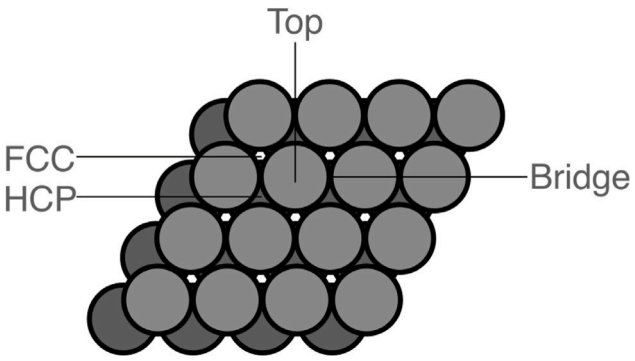

Fig. 1. Adsorption sites available on the Pt(111) surface. Platinum atoms are represented by gray spheres.

This study focused on systems with Li, Na and K adlayers on the Pt(111) surface, denoted here as Li/Pt, Na/Pt and K/Pt, respectively. The minimal coverage corresponds to a single alkali metal atom on Pt(111) within a (4×4) surface unit cell, leading to a coverage of $\Theta_{min} = 1/16$, or 0.06 ML. To model a 0.33 ML coverage, a $(2\sqrt{3}\times 2\sqrt{3})$ surface unit cell was employed. As possible adsorption sites, the top, bridge and two types of three-fold hollow sites, fcc and hcp, present on the Pt(111) were considered, as illustrated in Fig. 1.

By gradually occupying preferable surface sites with Li, Na and K atoms the systems at higher AM coverages were then created. The differential adsorption energy for each nth adatom was derived according to

$$E_{ads} = E_{nAM/Pt} - E_{(n-1)AM/Pt} - E_{coh,AM} \quad (1)$$

where $E_{nAM/Pt}$ and $E_{(n-1)AM/Pt}$ are the total energies of the systems comprising n and $n-1$ Li, K or Na atoms on the Pt surface, respectively, and $E_{coh,AM}$ is the cohesive energy per atom of the corresponding alkali metal. This "step-wise" adsorption energy allows to conclude how adding an atom to the adlayer affects its stability.

The bulk cohesive energy is obtained from the expression

$$E_{coh,AM} = \frac{E_{AM_n} - n \cdot E_{AM,g}}{n} \quad (2)$$

in which E_{AM_n} and $E_{AM,g}$ are the total energies of a cell with n AM atoms in bulk geometry and of one AM atom isolated in gas phase, respectively.

An alternative approach to estimate the stability of adlayers on the substrate is to calculate the integral adsorption energy [62] according to

$$E_{ads,i} = \frac{E_{nAM/Pt} - \left(E_{Pt} + n \cdot E_{AM,g}\right)}{n} \quad (3)$$

Here again, $E_{nAM/Pt}$ is the total energy of the system with a n AM atom adlayer, supported on Pt(111), $E_{AM,g}$ is the energy of the isolated AM atom and E_{Pt} the energy of the pristine Pt(111) surface.

The integral adsorption energy is the crucial quantity to determine the equilibrium coverage of the adsorbates as a function of their chemical potential [63,64]. It can furthermore be useful for estimating the contributions of the substrate–adlayer interaction, $E_{s\text{-}a}$ and adsorbate–adsorbate interaction, $E_{a\text{-}a}$ to the overall adsorption energy. The values of $E_{s\text{-}a}$ and $E_{a\text{-}a}$ can be obtained from:

$$\begin{aligned} E_{s-a} &= \frac{E_{nAM/Pt} - \left(E_{Pt} + E_{AM,adl}\right)}{n} \\ E_{a-a} &= \frac{E_{AM,adl} - n \cdot E_{AM,g}}{n} \\ E_{ads,i} &= E_{s-a} + E_{a-a} \end{aligned} \quad (4)$$

Here, additionally to the terms, described above, $E_{AM,adl}$ stands for the total energy of a free-standing adlayer (as it is referred to in the work

of Pašti and Mentus [62]) comprising n isolated atoms organized in a geometry identical to that they have on the Pt substrate.

The degree of strain allows to estimate how "compressed" or "stretched" the AM overlayer is due to the presence of the Pt substrate with respect to the corresponding bulk structure which can significantly influence the reactivity of metal surfaces [65,66]. It was calculated as indicated earlier in the literature [44,67]:

$$S = \frac{d_{AM-AM(adl)} - d_{AM-AM(bulk)}}{d_{AM-AM(bulk)}} \times 100\% \quad (5)$$

where $d_{AM-AM(adl)}$ and $d_{AM-AM(bulk)}$ are average AM-AM distances in adsorbed adlayers and in the bulk, respectively. From this formalism, positive values of S would correspond to a overlayer stretching, negative values–to its compression.

The work function, Φ, for pristine and adatom-modified platinum surfaces was calculated as the difference of the electrostatic potential in vacuum, V_∞, and the Fermi level of the surface, E_F:

$$\Phi = V_\infty - E_F \quad (6)$$

The adatom induced charge redistribution in the studied systems was analyzed using the Density Derived Electrostatic and Chemical (DDEC6) partitioning scheme [68,69], with net charges on atoms calculated with Chargemol [69,70]. The charge density difference, $\Delta\rho$, was obtained from the equation:

$$\Delta\rho = \rho_{AM/Pt} - \rho_{AM} - \rho_{Pt} \quad (7)$$

Here, $\rho_{AM/Pt}$ is the charge distribution in the system with an adatom on a Pt surface, ρ_{AM} and ρ_{Pt} are the charge distributions for the isolated alkali metal atom and the bare surface, respectively. Importantly, the charge density difference (CDD) must be calculated under the strict condition that the ρ_{AM} and ρ_{Pt} components of the studied systems are obtained using the same atom positions as in the composite system [71].

The obtained data were visualized by making a 2D slice through the three-dimensional representation of the charge density difference of each AM/Pt system. The cutting plane was selected in such a way that the obtained plane would include the adatom, the surface Pt atom directly in contact with it and another surface atom further away from the adsorbate (see Fig. S1). This allows to assess how the different surface atoms interact with the adsorbate depending whether they are in direct contact with it and to see the charge difference in a specific point where the adatom–surface interaction takes place.

The dipole moment per AM atom at all coverages with an adsorbate density n_o was determined using the Helmholtz equation that establishes a relation between the work function change, $\Delta\Phi$ and the dipole moment, μ [46,47,54]:

$$\mu = -\frac{\Delta\Phi}{2\pi n_o} \quad (8)$$

3. Results and discussion

3.1. Single Li, Na and K atom interaction with Pt(111)

3.1.1. Stability of the adatoms and preferred adsorption sites

The most stable adsorption site for each considered alkali metal was established by placing a single atom of lithium, potassium and sodium on all possible adsorption sites available on Pt(111) (Fig. 1) at an initial distance of ~2.5 Å with a subsequent relaxation of the systems. All AM species were found to preferably interact at the sites with the highest coordination, resulting in adsorption on three-fold hollow sites.

Specifically, the analysis of E_{ads} values revealed that for all adatom species the hcp site was the most stable one, followed by fcc (see Table 1). This is somewhat different from previously reported results [72,73], indicating that the fcc site was preferable for adsorption of single alkali metal atoms. However, from low-energy electron diffraction (LEED) structural analysis combined with theoretical calculations it was concluded that Na and K are more stable on the hcp site [46,47]. The authors also argued that the local electronic environment on the hcp sites leads to a more favorable overlap between the valence states of alkali metals and the Pt. As the result, even though the energy difference between fcc and hcp is very small (less than 0.1 eV as it can be seen in Table 1), the hcp sites enable a better screening of the alkali-induced dipoles and minimize the repulsive interaction with the underlying Pt layers. Overall, a common agreement on the preferable adsorption sites for AM is that the energy difference between hcp and fcc sites is negligible [72,74]. Since the experimental data suggests hcp sites as the most stable for Na and K at low coverages, they were chosen for the analysis of the Li, Na, and K interaction with Pt(111).

The values for the adsorption energy, listed in Table 1, point to a strong AM-Pt interaction. This is reflected by the fact that the listed E_{ads} that are determined with respect to the bulk cohesive energy of the AM (see Eq. (2)), are all negative indicating that the single AM atom adsorption on Pt(111) is energetically more favorable for the alkali atoms than joining the bulk structure of the respective bulk metal. This affinity for adsorption on Pt follows the order K > Na > Li, with sodium and lithium characterized by very close E_{ads} values.

The E_{ads} values calculated with respect to the isolated AM atoms are very close to those reported in earlier studies: −3.52 eV *vs.* −3.33 eV [73] for Li, −3.13 eV *vs.* −2.89 eV [73] for Na and −3.37 eV *vs.* −3.13 eV [73] for K. The difference between the calculated and reported values could be a result of different model parameters used in the present study and in the work of Matanović et al., the choice of the exchange–correlation functional and the AM coverage among them.

The distances between the AM and the substrate d_{AM-Pt} follow the same K > Na > Li trend, probably reflecting the decrease in the atomic radii (r_K = 202.5 pm, r_{Na} = 157.2 pm and r_{Li} = 122.5 pm [75]). It is evident that the weakest adsorbed lithium is closest to the surface, followed by sodium with an intermediate E_{ads} and then the most stable potassium. The adsorption of either of the AM species causes a small increase in Pt-Pt distances in the contact region from 2.80 Å to 2.85 Å, not affecting surface atoms further from the location of the adatom.

Interestingly, the E_{ads} values calculated with respect to the energy of an AM atom isolated in vacuum indicate a slightly different stability order of the AM stability as the one obtained using E_{coh} as the reference. This other trend, Li > K > Na, however, does not correlate neither with trends in the atomic numbers nor with adatom–substrate distances. This might indicate that E_{ads} calculated *vs.* E_{coh} provides a more accurate representation of the AM stability on platinum.

It must be noted here that in the study by Lehmann, Roos and Bertel [45] it was demonstrated that at coverages below Θ_{AM} = 0.22 ML the light alkali metals can be incorporated into the surface, reverting to regular adsorption at the higher coverages. In such systems the AM-AM repulsion would be mostly eliminated, which could be a stabilizing factor.

However, in the later works by Moré et al. the authors came to the conclusion that the subsurface K and Na adsorption in Pt(111) is not favorable especially at lower temperatures, mainly because of the size of Na and K atoms [46,47]. The insertion into the bulk of the Pt surface would cause a significant expansion of the internal structure of platinum, destabilizing the overall system. Furthermore, the formation of such systems would entail breaking of several stable Pt-Pt bonds and the creation of weaker AM-Pt bonds, which is another argument against the substitutional AM adsorption in Pt(111).

Nonetheless, the Li atomic radius is the smallest among the considered AM species, and the possibility of its insertion into Pt(111) surface was considered here as well, with the substitutional adsorption of Na and K taken as a reference. The analysis, described in detail in Section S1.1 of the Supporting Information, revealed that in all cases, the systems where one AM atom is inserted into the surface or subsurface layers of Pt(111) are less stable than the corresponding ones with AM atoms adsorbing on Pt(111) (Table S1), suggesting that

Table 1
Calculated cohesive (E_{coh}) and differential adsorption energies on hcp (E_{ads}^{hcp}) and fcc (E_{ads}^{fcc}) sites, distance between the adatom and the surface (d_{AM-Pt}), DDEC6 (**bold**) and Bader (*italic*) atomic charge values for adatom (Q_{AM}), average DDEC6 (**bold**) and Bader (*italic*) charges for Pt atoms in contact with it (Q_{Pt}) and adatom induced change in the work function ($\Delta\Phi$) for the studied AM/Pt systems.

System	E_{coh} (eV)	E_{ads}^{hcp} (eV)	E_{ads}^{fcc} (eV)	d_{AM-Pt} (Å)	Q_{AM} (e)[a]	Q_{Pt}[a]	$\Delta\Phi$ (eV)
Li/Pt	−1.68	−2.19	−2.10	2.01	**+0.75**/*+0.87*	**−0.31**/*−0.25*	−0.92
Na/Pt	−1.10	−2.24	−2.15	2.41	**+0.78**/*+0.82*	**−0.27**/*−0.22*	−1.46
K/Pt	−0.94	−2.60	−2.52	2.82	**+0.82**/*+0.84*	**−0.23**/*−0.20*	−1.97

[a] Negative and positive values correspond to charge gain and loss, respectively.

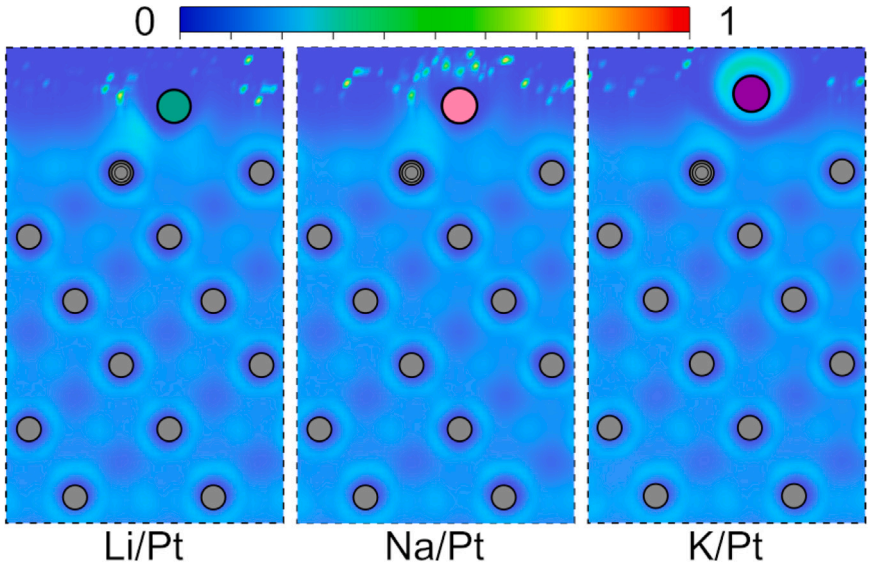

Fig. 2. 2D plots of the electron localization function for AM/Pt surfaces. The probability of finding electron varies from 0 (blue) to 1 (red). The gray circle with concentric inner circles represents the Pt atom in contact with the adatom, gray, green, pink and purple spheres denote Pt, Li, Na and K atoms, resp.

substitutional adsorption is less likely to occur than adsorption on the surface. Therefore, only adsorption of the AM on the Pt(111) surface was considered while studying the increasing coverage of Li, Na, and K.

3.1.2. Analysis of the electron localization function and charge density

The electron localization function (ELF) plotted in Fig. 2 was obtained by making a 2D slice through the three-dimensional representation of the electron localization data for each AM/Pt system (see Fig. S1). It indicates a small increase in the probability to find electrons in the contact region between the AM and platinum surface. The slightly smeared nature of this region points to the presence of mostly metallic bonds between all AM atoms and Pt. An interesting feature is seen in the K/Pt system, where the electron localization around the adatom visibly shifts away from the Pt surface, indicating a polarization of the adatom–Pt bond, not evident in the ELF plots for Li and Na. Overall however, the presence of the adatom appears to impact only Pt atoms directly in its vicinity, not involving either surface atoms located further away from the adsorbate or deeper in the bulk of the AM/Pt systems.

Charge transfer is an important aspect of the adatom–surface interaction. The determination of net atomic charges offers one of the simplest ways to assess the adatom-induced charge redistribution in adsorbate–surface systems in general and in AM/Pt systems in particular. In any material there is an electron cloud surrounding the atomic nuclei. The partitioning of a given charge distribution to specific atoms effectively means associating parts of this electron cloud to each atomic nucleus. Within this approach the net atomic charge will be defined as:

$$Q_X = Z_X - q_X \tag{9}$$

Here Z_X is the nuclear charge of atom X, and q_x – number of electrons attributed to this atom.

It is important to note that this assignment is by no means unique [76]. There are many approaches to assign fractions of electron clouds to a given atom, including the Hirshfeld [77], Bader [78], Charge Model 5 [79], and Density Derived Electrostatic and Chemical (DDEC6) [68, 69], partitioning schemes. Furthermore, net atomic charges can be estimated from a wave function using other methods, such as population analysis [80], and electrostatic fitting [81].

Consequently, net charges obtained for the same system using different approaches can vary significantly, and it is impossible to verify which method offers the most accurate results since partial charges are not accessible experimentally. Furthermore, population analysis methods are not directly applicable to plane-wave basis sets [82], and electrostatic fitting methods do not work for crystalline systems [83].

As for the partitioning schemes, the Hirshfield method usually underestimates net charges [79], and the Charge Model 5, while mitigating some shortcomings of the Hirshfield partitioning scheme by including empirical corrections to it, cannot be used to calculate certain atoms-in-materials properties [69].

For the AM/Pt systems both DDEC6 and Bader approaches to electron density partitioning agree that in all cases an adatom → surface charge transfer takes place. The adsorbed AM species become positively charged, while surface Pt atoms in contact with the adsorbates gain charge and become more negative, although both schemes yield different values of the partial charges for the AM and platinum atoms. Furthermore, within the DDEC6 method the derived positive charge values for the AM species decrease in the order K (+0.82 e) > Na (+0.78 e) > Li (+0.75 e), in agreement with the electronegativities of these elements: $\xi_K = 0.82$, $\xi_{Na} = 0.93$ and $\xi_{Li} = 0.98$ [84].

In contrast, the net atomic charges calculated for the same systems using the Bader approach yield a somewhat different trend, where positive values of Q_{AM} decrease in the row Li (+0.87 e) > K(+0.84 e) >

Na (+0.82 *e*). Importantly, neither of the partitioning schemes are able to describe accurately the exact relationship between the net charge transfer and change in the work function (see Table 1). However, the trend in charge transfer, predicted by the DDEC6 scheme, $Q_K > Q_{Na} > Q_{Li}$, correlates well with adatom-induced changes in the work function, $\Delta\Phi_{K/Pt(111)} > \Delta\Phi_{Na/Pt(111)} > \Delta\Phi_{Li/Pt(111)}$.

The overall more positive net charges derived with the Bader approach compared to those obtained with the DDEC6 partitioning could be the result of the reported tendency of the Bader charge analysis method to sometimes overestimate atomic charges, particularly in light atoms [85]. The disagreement on charge transfer trends, in its turn, arises from the fundamental differences in the partitioning schemes.

The Bader method is very sensitive to the local topology of the electron density, partitioning space into basins of the electron density, separated by zero-flux surfaces. The charge of each atom is estimated from the number of electrons contained inside its basin. For smaller atoms such as Li the valence density is concentrated close to their nuclei, and charge donation leads to a significant outward shift of the dividing surface, so that the Bader method assigns a more positive charge. Conversely, for larger diffuse atoms such as K, the valence density decays more gradually, so more electron density remains within their basin after adsorption, leading to a smaller apparent charge transfer.

In contrast, the DDEC6 approach partitions the total electron density into atomic contributions by optimizing the reference atomic densities to reproduce the electrostatic potential in the external region of the material, keeping the resulting charges chemically meaningful, *i.e.* charges on similar atoms in similar environments remain consistent [68,69].

Since both Bader and DDEC6 approaches predict a charge transfer from the AM adatoms to the platinum substrate, either of them can be used as the first estimate of the trends in charge transfer upon adatom–substrate interaction at different coverages. Taking into account that the final result cannot be verified experimentally, the choice of the scheme is, ultimately, subjective. Here the DDEC6 scheme was used since the charges obtained with it align better with trends in AM adsorption energies on Pt(111) and AM-induced changes in its work function. Furthermore, the DDEC6 method handles delocalized electrons better than the Bader scheme which is crucial for metallic systems [69].

The AM → Pt charge transfer was further confirmed by determining the spatial electronic distribution of the total charge density difference, $\Delta\rho$, from Eq. (7). As described in Section 2, a 2D slice was made out of the 3D charge difference representation (Fig. S2) with the cutting plane including the adatom, the Pt atom in contact with it and another surface atom not directly interacting with the adsorbed species (Fig. S1).

The obtained 2D slices can be seen in Fig. 3, which evidences that for all AM species only the two topmost layers of Pt are affected by the presence of the adatoms, while the charge distribution in the remaining four layers virtually remains the same as in the pristine surface.

In all AM/Pt systems a charge depletion region of roughly spherical shape is present above and on the sides of the adatoms, indicating the involvement of their *s* orbitals in the charge transfer process. At the same time, a charge buildup is seen at the Pt surface atoms in contact with the adsorbate, forming a region with one lobe oriented toward the adatom and another into the interior, indicating the involvement of the Pt *5d* orbitals [31,47] in the AM-Pt bond formation. Conversely, the charge density on the surface atom located further away from the interaction region does not undergo such a significant change as the Pt atom directly in contact with AM adatom, confirming the localized nature of the impact of the AM adatoms on the Pt electronic properties seen in the ELF plots (Fig. 2).

3.1.3. Changes in the work function of Pt(111) upon AM adsorption

The observed charge transfer should also result in a change of the work function, Φ, of the Pt(111) surface with the adsorbed AM atoms. The work function is an important characteristic reflecting the interaction of adsorbates with a catalyst surface and, hence, its reactivity [54,86,87]. For a given system the work function can be divided into contributions from the bulk part and from the surface. The bulk part of the work function corresponds to the position of the Fermi energy relative to the average electrostatic potential inside the bulk. Since it depends mainly on crystal structure, composition and electron density, it is practically not affected by the presence of the adatoms.

The surface component, in its turn, is very sensitive to the charge redistribution originating from the adsorption of species with electronegativities different from that of the atoms in the host surface. The presence of adatoms with electronegativities lower than that of Pt (ξ_{Pt} = 2.28 [84]) would lead to a positive surface dipole moment change, resulting in the decrease of the work function [18,31,54,88] from the calculated value of $\Phi_{Pt(111)}$ of 5.73 eV.

Fig. 4 summarizes the planar-averaged potential energy in AM/Pt systems as a function of the *z* coordinate. Notice that the number of minima on each panel corresponds to the total number of platinum layers in each system. Another important feature is the asymmetry of the potential energy values on the left and right sides of each plot, caused by presence of the adatom. It can be seen that in all cases the adsorption of the AM atom leads to a lowering of the potential energy and of the work function of the surface with the adsorbed AM atoms.

As seen in Fig. 4 and in Table 1, the biggest impact on the work function $\Phi_{Pt(111)}$ is seen for the potassium adatom, followed by sodium, whereas the lowest change was observed in the Li/Pt system. This trend follows the one seen for the total net charge values calculated for the adatoms (decreasing in the order K > Na > Li as discussed above) which is in agreement with experimental data available in literature, at least, concerning Pt with potassium and sodium adatoms [18,89].

As for Li/Pt, the calculated value for $\Delta\Phi$ is −0.93 eV, seemingly in disagreement with the value of −3.35 eV calculated for this system previously [72]. However, the latter $\Delta\Phi$ value was obtained for a lithium coverage of 0.25 ML, while the work function change reported here corresponds to a coverage of Θ_{Li} of 0.06 ML. Recalculating the work function for a 0.25 ML coverage yields a $\Delta\Phi$ value of −3.00 eV, significantly closer to the previously reported value.

Overall, the observed tendency of the AM adatoms to lower the work function of Pt are in line with previously reported studies on AM-induced Φ changes of transition metal substrates in general, and Pt in particular [18,46,47,89]. The reported work function lowering is usually attributed to the interaction between the valence state of the AM adsorbate and conduction band states of the transition metal substrate, resulting in an AM → substrate charge transfer.

3.1.4. Electronic structure analysis

Similarly to other systems comprised of Pt surfaces with foreign atoms on them, alkali metal adatoms can be potentially employed for a fine tuning of the catalytic properties of Pt-based systems, depending on the target process. However, comparing to adatom-induced $\Delta\Phi$ values for Pt(111) for other species upon single foreign atom adsorption at 0.06 ML coverage (−0.72 eV [31], −0.45 eV [31], and −0.45 eV [88] eV for Bi, Te and Ni, respectively) the effect of the alkali metals on the work function is the largest. For some processes this could deteriorate the Pt catalytic activity, as for the case of the hydrogen evolution reaction, where the AM-induced change in the work function would cause a stabilization of the reaction intermediate and hinder product removal from the surface, potentially leading to a blockage of active sites.

Despite the apparent simplicity of the AM/Pt systems, the interaction of Li, Na and K with Pt(111) involves a complex interaction of electronic states of the adsorbed species with the surface atoms. The

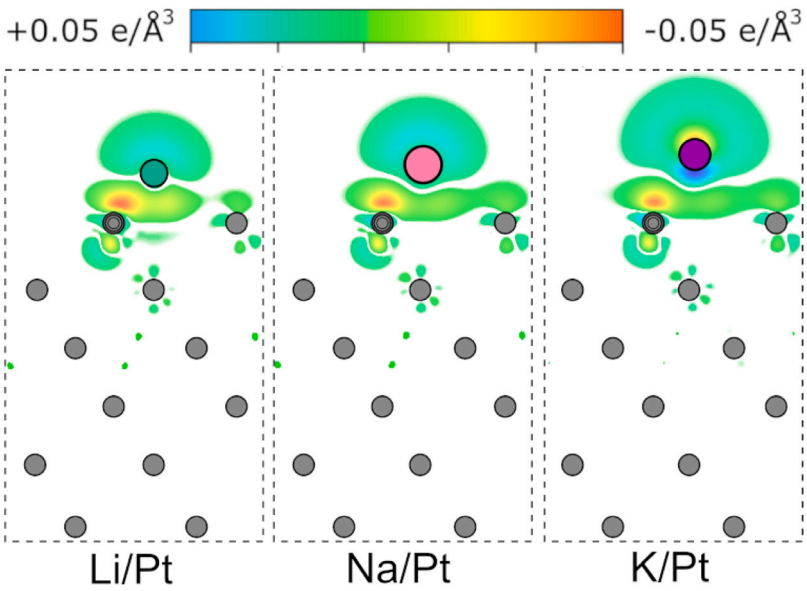

Fig. 3. Charge density difference plot for systems comprising a single atom of Li, Na, or K adsorbed on Pt(111). In each panel, the Pt atoms in contact with the adatoms are located on the left, while Pt atoms further away from the contact regions are located on the right. Red and yellow colors denote regions of charge buildup (negative partial charge), while blue and green of charge depletion (positive partial charge). The color coding of the atoms is the same as in Fig. 2.

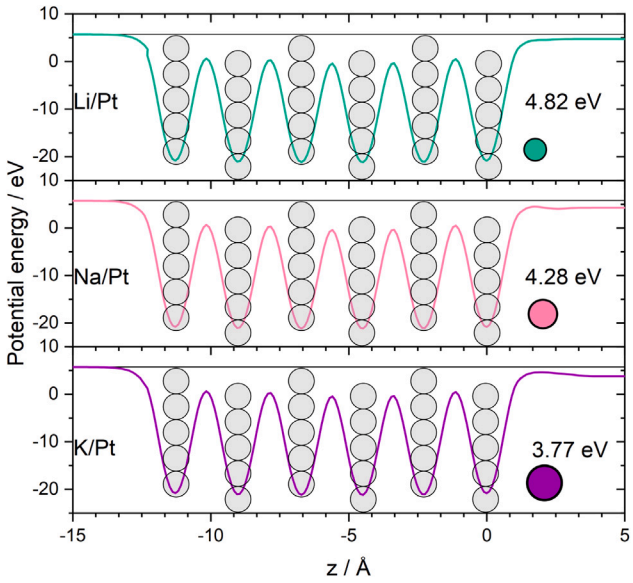

Fig. 4. Plane-averaged potential in the stable AM/Pt systems. Parts of the vacuum region on the clean side of each slab and on the side where the adatom is present have been cut out from each plot to facilitate the visualization. Gray, green, pink and purple spheres denote Pt, Li, Na and K atoms, resp. The horizontal black line in each panel indicates the work function of pristine Pt(111), 5.73 eV. The values of the work functions for the sides of the slabs with adatoms are indicated as well.

charge transfer by itself is not sufficient to fully understand the AM-Pt interaction, since it ultimately depends on the selected partitioning scheme. Thus, to further assess the mutual impact of the AM and Pt on their electronic structures an analysis was conducted of the changes in the *s* states of the AM species and in the *5d*, *6s* and *6p* states of Pt resulting from the AM-Pt interaction. This analysis could be especially useful when identifying the orbitals of the adatoms and of platinum that were involved into charge transfer and AM-Pt interaction.

For this purpose the difference between the *s* states of the adsorbed AM and the states of the isolated species was analyzed, as presented in the upper panel of Fig. 5. As for platinum, the effect of the AM presence was estimated from the difference between the *s*, *p* and *d* states of the surface atom interacting with the AM adatom and the states of the corresponding Pt atom in the bare surface. The most affected states are summarized in the bottom panel of Fig. 5. Also changes in all states of platinum atoms in the contact region are illustrated in Fig. S3 of the Supplementary Information. The specific choice of the surface atoms in the direct vicinity of the adsorbate was dictated by the fact that surface atoms further away from the modification site do not undergo any significant changes in their electronic structure as evidenced from the ELF and CDD plots, and, therefore, are not involved in the AM-Pt interaction.

It is evident that a depletion was found in all cases for the AM *s* states. For Li and Na the depopulation of their *s* states is comparable, while for K the observed *s* state depopulation was significantly higher, in agreement with the charge transfer tendencies discussed above. The observed disappearance of the states in the vicinity of the Fermi level has been already reported for lithium upon its adsorption on Pt(001) [72], suggesting the possibility that Li, Na and K suffer similar changes in their electronic structure upon adsorption on Pt surfaces with different orientations.

As for platinum, the presence of any AM affects all electronic states of the surface atom in the vicinity of the adatom, although some states were affected more than others. Specifically, the biggest changes were seen in the d_{z^2} and d_{xz} states, followed by the much less affected *s* state, regardless of the nature of the AM adatoms. The changes of the d_{xz} state apparent in Fig. 5 corroborate the preliminary conclusions made from the CDD plot in Fig. 3 about its involvement into the AM-Pt bonding.

Changes in the rest of the states are rather small, allowing to draw the conclusion that the interaction of the AM adatoms and Pt mainly involves the *s* states of the adsorbates and the d_{z^2} and d_{xz} states of platinum. Similar results have been already reported for the electronic states of Pt in the Na/Pt(111) system [47], where the adatom-induced polarization of Pt atoms *via* filling of d_{z^2} orbitals and the depletion of $d_{xz,yz}$ states was argued to contribute to the strong interaction of Na and Pt in particular and of smaller alkali metals with transition metal substrates in general. The obvious similarities in the electronic structure changes seen for all AM/Pt systems, regardless of the nature of the adatom, suggests the applicability of this conclusion for Li and K as well.

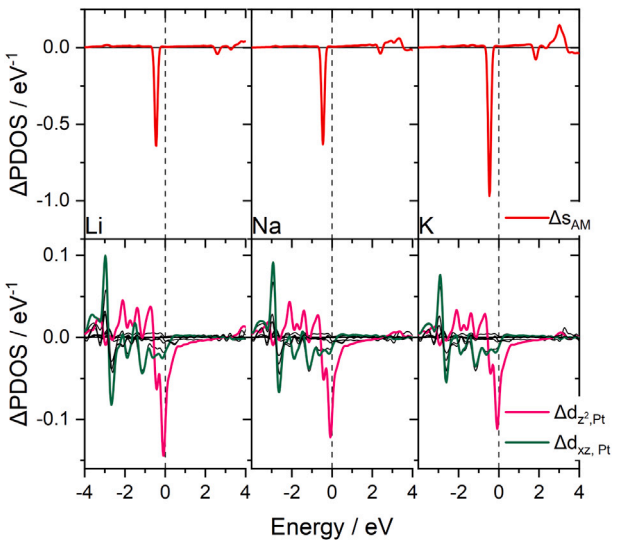

Fig. 5. Changes in the projected densities of states (PDOS) of AM species and Pt upon AM adsorption on Pt(111). For clarity the range of energies between −4.0 eV and 4.0 eV is shown. The orbitals, contributing to charge transfer are indicated: *s*-orbitals of AM with red; d_{z^2}- and d_{xz}-orbitals of Pt with pink and green. Thin black lines denote the orbitals of Pt that do not undergo a noticeable change upon the AM adsorption. Dashed vertical line indicates position of the Fermi level.

These findings paint a picture, similar to that observed for the evolution of electronic states of Pt upon adsorption of a single atom of Bi and Te, where the adsorption process affected the electronic states of the substrate atoms that extended toward the perpendicular direction of the surface, causing only little changes in the rest of the electronic states [31]. Indeed, the d_{z^2} state is oriented directly perpendicular to the surface plane while the lobes of the d_{xz} one have an angled orientation above and below the plane, contributing to the adsorption on the hcp three-fold hollow sites, where the adatom and the surface atoms involved into the AM-Pt interaction form a tetrahedron-like geometry.

3.2. Formation and properties of 2D layers of Li, Na and K on Pt(111)

3.2.1. Structural characteristics of the planar AM adlayers and adsorption energy trends

The AM adsorption on Pt(111) at low coverages leads to a strong repulsive interaction between the adsorbed species because of the large dipole moment associated with their adsorption [18,43,44,46,47]. However, while the formation of uninterrupted AM islands on the surface is not possible because of the electrostatic repulsion between the dipoles, the cohesive adatom–adatom interaction potentially could overcome it. Therefore, the coadsorption of two AM atoms at the lowest coverage of 0.13 ML was first considered on the neighboring hcp sites ($d_{AM-AM} \approx 3.5$ Å) and on hcp sites separated by two atomic rows ($d_{AM-AM} \approx 5.6$ Å).

The results for these arrangements revealed that the Na/Pt and K/Pt systems with two adatoms initially placed on neighboring hcp sites are energetically extremely unfavorable. As a consequence, upon allowing for relaxation, the adatoms moved to the hcp sites at a distance of 5.6 Å. As for Li/Pt, the adatoms remained on the neighboring surface sites, however, this arrangement is 0.2 eV less stable than the system with adatoms adsorbed at a larger distance. Subsequently, a higher population of the Pt(111) surface with adatoms was achieved, when possible, by placing each new AM atom at the maximum distance from the atoms already present on the surface.

Importantly, for a Na and K coverage of 0.25 ML (2 × 2) structures have been reported [46,47] with significant separations between coadsorbed adatoms. However, higher coverages could give a rise to alternative adatom arrangements, including different adatom in-plane distributions and aggregations. Therefore, for coverages above 0.25 ML several alternative 2D structures have been tested, and these calculations confirmed that the structures, reported in the present work, correspond to the lowest-energy configurations.

Another possible consequence of the strong AM-AM cohesive interaction could be the adsorption of AM atoms on the atoms of the same species already adsorbed on the surface and the formation of 3D structures. The possibility of a two-dimensional layer formation of a given metal on a substrate can be assessed by comparing the adsorption energies of the adatoms with their corresponding bulk cohesive energies that can be obtained from Eq. (2). Specifically, for adatom–substrate systems, in which the adsorption energy, E_{ads}, calculated from the Eq. (1) using E_{coh} as a reference, is equal or more positive than 0 eV, the adatoms will preferably bind to each other and form 3D structures. In the case when E_{ads} remains negative, the adatom will preferably interact with the substrate, forming a planar 2D structure. The values for E_{ads} and E_{coh}, listed in Table 1 for the lowest considered coverage of 0.06 ML indicate that initially all considered AM species will readily interact with the Pt substrate.

Importantly though, with growing adatom coverage the value of E_{ads} for a given AM may become more positive, and if at a given coverage it becomes equal or larger than 0 eV, the formation of a 3D geometry will be energetically more favorable from then on. Therefore, the $E_{ads} < 0$ criterion was used for all AM coverages to assure that the overlayer maintained its planar structure.

Also, at high enough coverages, even though the condition of negative E_{ads} is fulfilled, the surface could become too crowded and would not be able to accommodate the next adatom into the 2D structure, making a 3D geometry the only option. Thus, for coverages equal or greater than 0.31 ML, the stability of 2D structures was compared to that of possible three-dimensional geometries with identical number of adatoms in the system to assure that the planar adlayer was more stable than the 3D structure with the same number of AM atoms in it. The results evidenced no formation of 3D structures in the range of coverages up to maximum coverage specific for each considered AM, discussed further.

With this in mind the AM adatoms were placed one by one onto the hcp sites of the Pt(111) surface at increasing Θ_{AM} and were allowed to relax. The obtained stable geometries are summarized in Fig. 6, the corresponding evolution of the adsorption energy values with the coverage is shown in Fig. 7. It is evident that at lower coverages of 0.13 ML and 0.25 ML, the surface has enough sites for the adatoms to maintain the maximum separation due to repulsive interaction. At these coverages the average adatom–adatom distance is mainly defined by the distance between the surface hcp sites and for all AM species it is close to 5.6 Å, leading to p(2 × 2) pattern, reported previously for Na and K on Pt(111) [43,46,47]. The degree of strain, calculated for Li, Na and K from the Eq. (5) at these low coverages was +87 %, +54% and +22%, respectively, indicating a significant stretching of the AM adlayers compared to the bulk structure of the adsorbed metals.

At coverages higher than 0.25 ML, the surface becomes more crowded and the adsorbed species are not longer able to remain on the sites that are energetically preferable at lower coverages. For instance, at $\Theta_{AM} = 0.33$ ML 4 adatoms on the $2\sqrt{3}\times2\sqrt{3}$ surface are occupying the hcp sites that are separated from each other by a single fcc site, rather than by unoccupied hcp site as at the 0.25 ML coverage (see Fig. 6). Thus, while the AM adatoms are also organized in a rhombus-like pattern at the 0.33 ML coverage, the AM-AM distances are close to 4.8 Å. As the result the AM adlayers are less stretched than at the 0.25 ML coverage: +61%, +32% and +4% for Li, Na and K, respectively.

Further increasing coverage leads to the surface getting more populated by the adatoms, however, up to $\Theta_{AM} = 0.50$ ML, the overlayers'

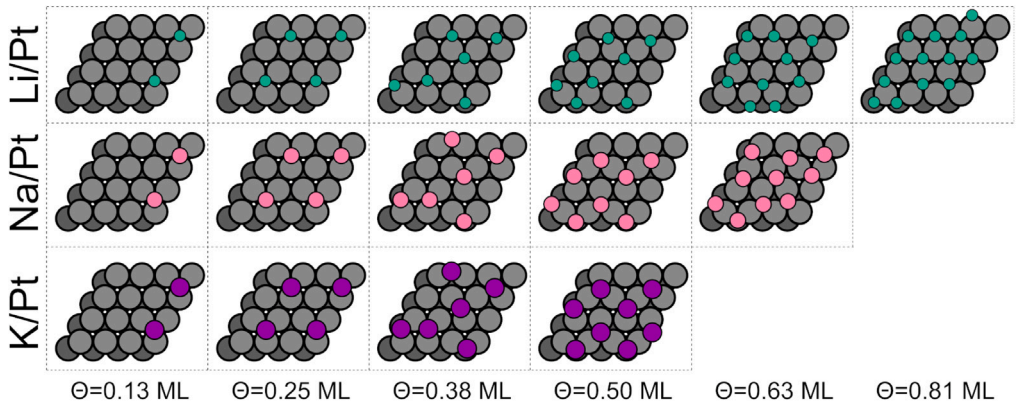

Fig. 6. Stable geometries for selected coverages of Li, Na and K on Pt(111) up to Θ_{AM} values at which the adlayer maintains 2D structure. Gray, green, pink and purple spheres represent Pt, Li, Na and K atoms, resp.

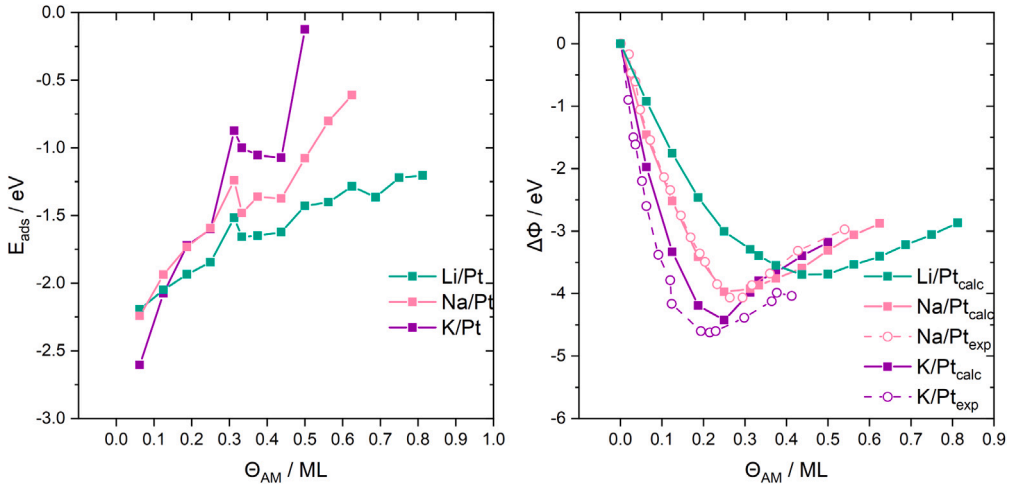

Fig. 7. *Left panel:* Differential adsorption energies for Li, Na and K on Pt(111) for the range of coverages where the adlayers maintain 2D structure. *Right panel:* Calculated changes in the work function for Pt(111) upon Li, Na and K adsorption in the same range of coverages.

structures remain very similar. At this coverage, the geometry of the adlayer has a hexagonal organization, largely defined by the substrate's geometry, because the AM-Pt interaction strength is able to overcome the repulsive AM-AM interaction, possibly resulting in an effective emerging cohesive AM-AM interaction. The resulting overlayers, however, are noticeably compressed, as seen from the calculated degrees of strain of +1% for Li, −16% for Na and −31% for K. In all cases the growth of the adlayer up to the half-monolayer coverage has gone through continuous compression, rather than *via* the formation of islands, which confirms a defining role of the electrostatic repulsion in this process at coverages that are lower or equal to 0.50 ML.

As it can be seen, the overlayer of potassium is significantly more compressed than adlayers of Li and Na, mainly because of its atomic radius being larger than of the rest of the considered AM (r_K = 202.5 pm, r_{Na} = 157.2 pm and r_{Li} = 122.5 pm [75]). As a result, at coverages higher than 0.50 ML no K adlayer with 2D structure is formed, making the half-monolayer coverage the highest possible for potassium layers on Pt(111) to maintain planar geometry.

For Li and Na, however, this is not the case, and at Θ_{AM} = 0.63 ML their adlayers still retain a 2D geometry. A closer look at Fig. 6 evidences that Li and Na adatoms still are organized in a pattern close to hexagonal, which is more symmetrical for Li than for Na, where a slight distortion is seen, due to the higher compression of the latter (−12% for Li and −23% for Na).

At coverages higher than 0.63 ML, Na no longer forms two-dimensional layers on Pt, rather interacting with sodium adatoms already present on the surface. Lithium, in turn, is able to reach a significantly higher coverage of 0.81 ML after which the two-dimensional adlayers do not form anymore. At Θ_{Li} = 0.81 ML, corresponding to 13 Li atoms per surface unit cell adsorbing mainly on the hcp sites, a 2D structure is formed with hexagonal symmetry. Because of the lattice mismatch between the Li adlayer and the Pt substrate the adsorbed layer is significantly compressed as evidenced by −16% of strain.

Overall, the critical compression, S_{crit}, after which only three-dimensional AM structures form on Pt(111) are specific for each adsorbed metal. The lowest one of −16% was estimated for Li at Θ_{Li} = 0.81 ML, followed by Na at Θ_{Na} = 0.63 ML with S_{crit} = −23% and the largest one of −31% calculated for K at half-monolayer coverage.

A direct comparison of the obtained maximum AM coverages with experimental data is complicated, because most of the studies report ordered AM overlayers on Pt(111) at Θ_{AM} = 0.25 ML with (2×2) structure or at Θ_{AM} = 0.33 ML with $(\sqrt{3} \times \sqrt{3})R^o$ geometry. However, several works have investigated higher AM coverages on Pt(111) and on selected other surfaces [89–92], and maximum coverages for Na and K on Pt(111) reported in an experimental study were $\Theta_{Na} \approx 0.55$ ML and $\Theta_K \approx 0.42$ ML [89], close to theoretical values of 0.63 ML and 0.50 ML, resp. obtained in the present study. Larger calculated values can be attributed to imperfections in practical surfaces and experimental conditions that are different from those within the DFT model.

Looking at the evolution of E_{ads} with coverage, illustrated in Fig. 7, the overall tendency of E_{ads} to become more positive with coverage, is evident. This trend is exactly opposite to the stabilization observed

for metals with attractive interaction in their adlayers, supported on Pt(111), such as Pd, Pt and Ni [62,88].

Also, regardless of which AM is present on the surface, two main regions can be distinguished on the plot: the first one corresponding to the range of coverages between 0.06 ML and 0.25 ML, the second one — to Θ_{AM} between 0.31 ML and maximum coverage where each AM overlayer maintains a planar geometry.

In the first region the adsorption energy is becoming more positive (AM-Pt interaction weakening) rather monotonously for each AM species. This effect is the biggest for K, followed by Na, and the lowest E_{ads} change is seen for Li, indicating that the addition of each new atom has an effect on the stability of the adlayer decreasing in the row of K > Na > Li. This can be tied to the atomic radii of these metals decreasing in the same order. Taking into account that AM atoms are larger than late *d* transition metals, such as Pd, Pt and Ni, it can be argued that at higher coverages the large size of the AM adatoms is one of the important factors driving adsorption properties of the AM species on Pt, giving rise to the repulsion of the atoms in the adlayer.

At the AM coverage of 0.31 ML a distinctive feature is seen on the plot, corresponding to a sudden weakening of the AM-Pt interaction (jump of the adsorption energy toward more positive values), followed by the stabilization of the adlayer until it reaches half-monolayer coverage. After that the adsorption energy values for the AM again become more positive with each added atom until reaching the last coverage where 2D adlayer is formed.

This feature appears because at 0.25 ML coverage the 4 AM adatoms present on the surface are able to adopt the geometry that assures their maximal separation, as seen from the degrees of strain, discussed above. Inclusion of the fifth atom destabilizes this structure significantly, leading to the "bump" in the E_{ads} *vs.* Θ_{AM} plot. It can be argued that the following stabilization can be the result of the compression of the adlayer and cohesive AM-AM interaction in it that contributes to the overlayers' stabilization on a substrate [88]. Also, at the 0.33 ML coverage the AM adatoms adopt a rhombus-like geometry with an average AM-AM distance of 4.8 Å as discussed above, thus forming a more stable adlayer than at 0.31 ML coverage. However, once the surface becomes more crowded the AM adlayers continue to be destabilized as seen in Fig. 7.

3.2.2. *Work function and dipole moment coverage-dependent trends*

The AM adatoms lower the work function of the surface due to charge transfer, as described above. This tendency is preserved at higher Θ_{AM} as well, as can be seen in Fig. 7. It is evident that for Na/Pt and K/Pt the obtained dependency of $\Delta\Phi$ on the AM coverage agrees very well with previously reported experimental trends [18,44,89], while for Li/Pt, to the best knowledge of the authors no such data has been reported so far. For each added AM atom, the work function first decreases, reaching a minimum after which it increases until the formation of the 2D adlayer is no longer possible.

While all considered systems have these features, regardless of the adsorbed AM, the effect of each added atom on the value of Φ is the biggest in the K/Pt system, followed by Na/Pt and Li/Pt. The position of the minima of the curve is also specific for each AM species: for K and Na the work function starts to increase after reaching Θ_K of 0.25 ML, while for Li this change occurs at a higher coverage of 0.44 ML. It is unclear whether the work function would continue increasing at higher coverages or it would reach a plateau, similarly to Bi/Pt(111) [33] or Na/Ni(100) [93], since monolayer and higher coverages were not considered in the present study. It is also possible to assume that at multilayer AM coverages the work function of the AM/Pt systems will be approaching the value of the AM surface, since sufficiently thick metallic adlayers would have properties resembling those of the parent metal [94], in particular when the growth is no longer pseudomorphic.

A work function passing through a minimum with increasing coverage of metal adlayer on a metal substrate has been reported before for systems such as Pd, Pt, Cu, Au, Pb and Bi on Pt [33,62]. This

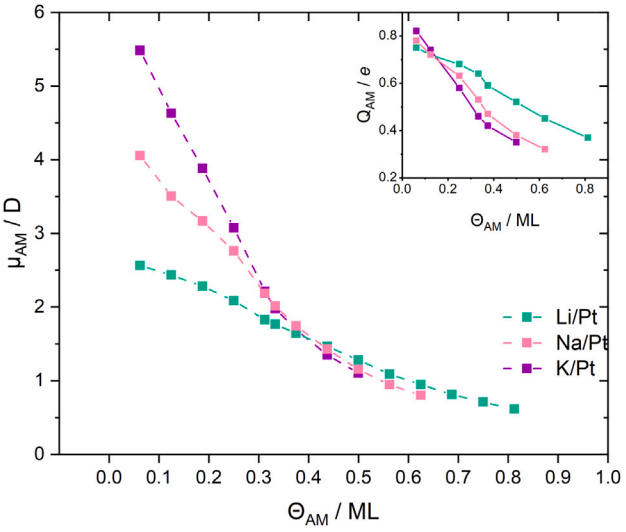

Fig. 8. Dipole moment as a function of the AM coverage, calculated from Eq. (8). The inset graph summarizes average atomic charges for each AM at selected coverages.

phenomenon has been explained by the depolarization of the adsorbate with growing coverage [44], which in turn could be the result of the back donation of charge from substrate to adlayer [62]. If this is the case for the AM/Pt systems, one way of confirming it is analyzing the evolution of the AM dipole moments with their growing coverage.

Fig. 8 summarizes the changes in dipole moment per adsorbate atom at each studied coverage and the net atomic charges for selected Θ_{AM}. In agreement with the observations made from the ELF plot in Fig. 2, the K adatom has the highest dipole moment, followed by Na and Li. These high dipole moments at low coverages also lead to a significant repulsive AM-AM interaction even when there are only two AM atoms simultaneously present on the surface. The decreasing dipole moments as a function of AM coverage points to an universal depolarization of the considered AM adatoms, in agreement with the data on Na and K adlayers on metal substrates [43,44]. It must be noted here that net atomic charges values for each AM decline with the coverage, evidencing a decrease in the AM-Pt interaction that is in agreement with differential adsorption energies gradually growing more positive in the same range of Θ_{AM} (Fig. 7).

Combined with the net positive charge decreasing with the growing coverage, the depolarization of the overlayers indeed can be the reason behind the AM/Pt work function shape seen in Fig. 7. Importantly, these factors also lead to a decrease of the AM-AM repulsive interaction with growing Θ_{AM}, making the binding of higher number of the AM in a 2D geometry possible, instead of pushing them to form a two-layer structure, as it is seen in case of halide adsorption on Pt(111) [54].

The coverage-induced changes in the interaction of the AM atoms within the overlayers and with the substrate can be visualized by employing the integral adsorption energy and its decomposition into substrate–adlayer interaction, $E_{AM\text{-}Pt}$, and adsorbate–adsorbate interaction, $E_{AM\text{-}AM}$, in the same adlayer (see Eqs. (3) and (4)), summarized in Fig. 9. It can be seen that, first of all, the comparison of the integral adsorption energy with the cohesive energy cannot be used as a criterion for the formation of a metal adlayer with planar geometries because the $E_{ads,i}$ values calculated for the AM adlayers with 3D structures still remain well below the corresponding cohesive energies.

Nonetheless, these plots illustrate the tendencies for substrate–adlayer and adsorbate–adsorbate interactions, described above. Specifically, it can be clearly seen that at low coverages the main contribution to adsorption energy comes from Pt interacting with the adatoms,

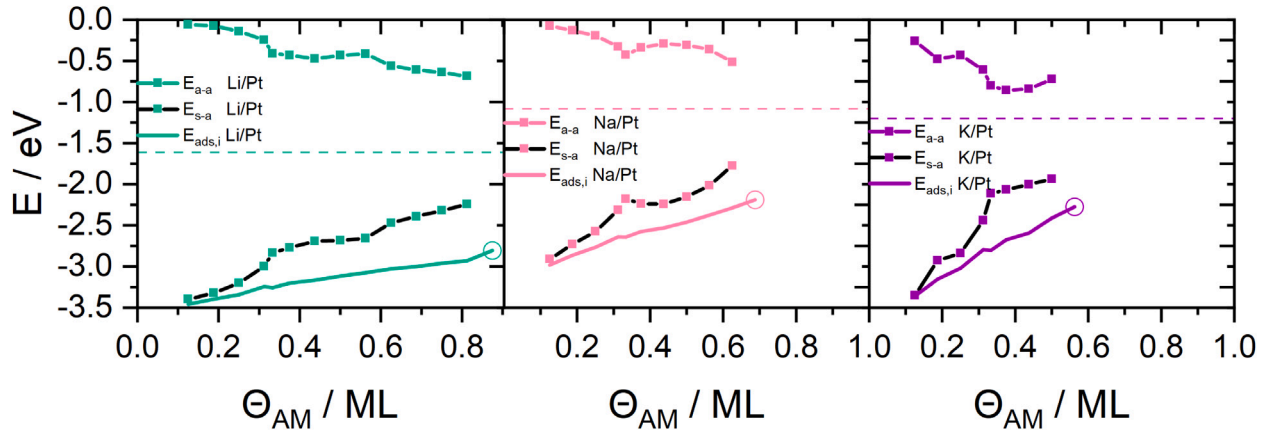

Fig. 9. Integral adsorption energy $E_{ads,i}$ and its $E_{AM\text{-}AM}$ and $E_{AM\text{-}Pt}$ contributions, calculated as in [62] in the range of considered Θ_{AM}. $E_{ads,i}$ values for Θ_{AM} where the adlayer has 3D geometry are included as well and denoted by circle on each plot. Horizontal dashed lines indicate cohesive energy for each AM species.

while the AM-AM interaction is very close to 0, due to the significant separation of the adatoms on the surface.

As coverage increases, an adlayer depolarization occurs and the adatom–adatom interaction becomes energetically more favorable while the AM-Pt contribution to the overall adsorption energy decreases, and its values become more positive with growing Θ_{AM}. Thus, when there are only few AM atoms present on the Pt(111) surface they mainly interact with the substrate. At higher coverages, the adatom–substrate decreases, in agreement with net atomic AM charges declining with the growing Θ_{AM}, and the adatom–adatom interaction within the adlayer plays gradually increasing role, resulting in destabilizing of the adsorption of the adlayer.

In this regard, it must be noted here that while the curves for $E_{AM\text{-}AM}$ changing with Θ_{AM} in Fig. 9 seem to go toward negative values in the opposite mirror fashion to that of $E_{AM\text{-}Pt}$, a careful revision shows that the decrease in the adatom–substrate interaction energy is more than twice as large as the increase in the adatom–adatom interaction energy in the adlayer, which is especially evident in case of the K/Pt system. This difference shifts the overall balance between these energies toward destabilization of the overlayer adsorption.

Overall, the obtained results identify the combined effect of the interaction of the adsorbed atoms with the underlying substrate and the mutual interaction of the AM atoms in the adlayer as an important factor driving the formation of the adlayer. It is largely defined by the charge transfer from the AM to Pt that gradually decreases with growing coverage leading to the depolarization of the AM overlayers. As a result, an attractive AM-AM interaction becomes possible, contributing to the stabilization of the adlayer with planar geometry.

3.3. Platinum surfaces modified with alkali metals in context of catalysis

3.3.1. Effect of structural and fundamental changes in AM/Pt surfaces on their catalytic activity

The exact understanding of the factors in control of the reactivity of a material toward a specific heterogeneous reaction is one of the most challenging goals of surface science in general and of informed novel material design in particular. From the results obtained in the present study it can be seen that the adsorption of the AM on Pt surfaces causes significant structural changes in the resulting systems. Combined with the complex interplay of the electronic states of the adatoms and Pt surface atoms, these changes could give rise to a shift in the catalytic properties of the complex AM/Pt systems, which must be carefully analyzed.

In this regard, at lower AM coverages, Pt sites not eclipsed by the adatoms will be still available for interaction. Their fundamental properties, however, will be affected by the present overlayer and they would be expected to interact differently with possible adsorbates compared to surface atoms of a pristine Pt(111).

For instance, an experimental study showed that the presence of potassium on platinum stabilizes adsorption of CO on top and bridge sites of the surface [18]. Another experimental study investigated the coadsorption of water with K and Na on Pt(111), and although not specifying adsorption sites for H_2O, indirectly argued for H_2O interaction with Pt-sites [89]. This work also demonstrated that the presence of K promotes H_2O dissociation due to dipole–dipole interaction between the coadsorbed species causing water molecule reorientation. This promoting effect depends on potassium coverage, thus evidencing the importance of the combination of electronic effects and AM-induced structural factor on catalytic properties of platinum.

At higher Θ_{AM} there will be no clean Pt-sites available for interactions with possible adsorbates as it can be seen in Fig. 6. It can be surmised that in this case any possible adsorbates approaching the surface will be interacting mainly with the AM-sites. Importantly, these sites cannot be treated simply as those on a corresponding AM surface, since the AM-Pt interaction modifies fundamental properties of both overlayer and substrate species. Instead, the AM/Pt systems must be considered as unique materials with properties different from their parent systems [94]. To the knowledge of the authors, however, no experimental or theoretical data are available specifically on the interaction of AM-sites with other adsorbates, thus making it impossible to predict adsorption trends, which could potentially present an interesting topic for future studies.

On the other hand, the obtained results demonstrate that AM adsorption on Pt(111) produces two key electronic effects: a charge transfer from the AM adlayers to the Pt substrate and a noticeable lowering of the surface work function. The significance of these effects on catalytic properties of Pt can be easily seen in the context of CO_2 reduction.

Clean Pt(111) in ultra high vacuum (UHV) does not bind CO_2 in the range of temperatures between 100 K and 300 K, however, doping platinum with potassium enables CO_2 adsorption and dissociation [19]. This could be attributed to the AM-induced lowering of the work function, discussed above, which would activate CO_2 by facilitating electron donation into its antibonding π^* orbitals from the surface. Indeed, Liu et al. argued that on the K/Pt surface CO_2 is adsorbed in two forms: weakly-bonded CO_2 and activated CO_2^- that consequently dissociates into CO and O^-. Similar conclusions can be made for experimentally observed potassium-promoted CO_2 dissociation on metals such as Ag [20] or Cu_xO/Cu(111) where activation of adsorbed CO_2 was evidenced as well [21].

Another study directly established the correlation between the promoting effect of alkali metals on the catalytic properties of copper toward water gas shift reaction [95]. It was revealed that the promoting

AM effects on H_2O and CO_2 dissociation on copper increases in the order of Cs > Rb > K > Na, opposite to the electronegativity trend of these metals Na > K > Rb > Cs. It was demonstrated above that less electronegative alkali metals donate more electrons to the same substrate (see Table 1) and are responsible for the higher work function change and larger surface dipole moment. Thus, less electronegative AM adatoms would promote more electron donation from the substrate to H_2O and CO_2 on the same surface, activating them and lowering dissociation barriers to a larger extent, compared to more electronegative AM adatoms. In agreement, the resulting dissociation barriers for water and carbon dioxide on Cu(111) follow the trend of the AM electronegativities, Cs/Cu(111) > Rb/Cu(111) > K/Cu(111) > Na/Cu(111) > Cu(111) with the highest barrier on pristine Cu surface.

Because the CO molecule is very stable, no dissociation is seen on Pt(111) under typical conditions even with AM present on the surface [18]. Nonetheless, CO coadsorbed with AM on Pt(111) desorbs easier compared to CO on pristine platinum, reducing surface poisoning [17]. Similarly to CO_2 activation the effect of alkali metal adatoms on the CO stability can be attributed to the work function decrease and facilitated electron donation from platinum to $2\pi^*$ orbital of CO. In agreement with this, a theoretical study on the adsorption and activation of CO on clean and potassium-modified transition metals, including both non-noble and noble ones, revealed that the addition of the potassium atom to the studied surfaces can promote CO activation on Fe(100), Ni(100), and Pd(111) surfaces [96]. Also, potassium was reported to universally stabilize CO, which was attributed to the strong short-range K → CO charge transfer. While somewhat disagreeing with the experimental data, this work evidenced the extreme importance of the electronic effect of potassium on CO activation on transition metals surfaces.

The importance of charge redistribution induced by the presence of potassium on metal surfaces could be also seen in the context of extremely important reactions, such as the Haber-Bosch process. It has been studied extensively and widely implemented on the industrial scale requiring, however, high temperature and pressure. A practical implementation of a low-temperature, low-pressure process still remains elusive because the active sites of industrial catalysts are poisoned by oxygen or hydroxyl groups at low temperatures. The industrial Haber-Bosch process heavily relies on a catalyst which is typically iron with potassium and oxygen-containing promoter [14]. Therefore, a theoretical study has been conducted to investigate the role of potassium on the catalytic properties of rhenium, ruthenium, iron, rhodium, and platinum toward the Haber-Bosch reaction [97]. In agreement with the results discussed above, it was reported that the potassium presence on metal surfaces has the two-fold promoting effect: because of dipole–dipole interactions electropositive potassium stabilizes the partially negatively charged transition N_2 state and promotes N-N bond scission through enhanced electron donation from metal. At the same time the presence of potassium destabilizes NH_2, facilitating its evacuation from the surface and increasing the reaction rate. The side effect of this is oxygen stabilization on the surface, that on practice is mitigated by higher temperatures.

The electronic effects of the considered alkali metals adsorbed on the metal substrate cannot be directly tied to the reported AM-promoted electrocatalytic activity of various metals toward CO_2 and O_2 reduction, alcohol electrooxidation or hydrogen evolution reaction, because AM do not adsorb specifically on metal surfaces in electrochemical conditions and instead exist in the form of hydrated cations. Still, in many cases the impact of the AM on catalytic properties of complex electrochemical systems can be traced back to the tendencies discussed above. For instance, the enhanced CO_2 reduction on Cu and Au [6,7] was attributed to a dipole field formation due to the presence of alkali metals in solution. This field stabilized the adsorption of surface intermediates with significant dipole moments, at the same time decreasing the energy for CO_2 adsorption and facilitates the formation of C_2 products. Still, it is evident that a better fundamental-level understanding of the AM/Pt materials in presence of water is essential for clarifying the impact of the AM cations on catalytic properties in the practical systems. In this regard, *ab initio* molecular dynamics methods or deep neural network models, such as those employed in Deep Potential Molecular Dynamics [98] can offer a important insight into factors affecting fundamental and catalytic properties of these systems.

Overall, the obtained results clearly align with experimental data available on the AM overlayers supported on metal surfaces and their catalytic properties. Understanding composite adatom–substrate systems is not a trivial task and it requires more data to become a valuable and reliable tool for a systematic design of catalysts with an optimal set of characteristics tuned for the target processes. Thus, the present study contributes to the field of the informed design of Pt-based materials and offers possible directions for the further research on the AM/Pt systems.

3.3.2. Interaction of AM adlayers with Pt(111) compared to that of halides

In real-life systems, an electrolyte interacting with a given electrode surface contains equal number of cations and anions. Often, the anions that are present in the system are halides, such as Cl^-, Br^-, and I^-. Because of their strong interaction with metals, the electrodes become covered with halides in the course of many electrochemical processes, leading to a noticeable changes in their fundamental properties, directly related to catalytic performance [54].

Thus, by carefully comparing similarities and differences in adsorbate-induced shift of platinum properties upon interaction with AM atoms and with halides [4,54], could provide a better understanding of a complex phenomena taking place on metal electrodes when AM cations and halide anions are simultaneously present in electrochemical solution.

In this regard, it has been clearly demonstrated above that AM adatoms form mostly metallic bond with Pt substrate, ceding charge to it, while the halides bonding with platinum has more covalent nature, and is accompanied by charge transfer toward the adsorbate. Regardless of the nature of the bond, a repulsive adsorbate-adsorbate interaction is seen in the AM adlayers and overlayers of halides on Pt(111), leading to maximum separation between adatoms at each given coverage.

Also, both types of the adsorbates lower the work function of Pt(111), although the mechanisms behind this change are different. The AM adatoms lower the work function due to the AM → Pt charge transfer and resulting positive surface dipole change. On the other hand, for halide adsorbates the charge transfer from the surface would be expected to increase the work function. In reality, however, this effect is overcompensated by a significant polarization of the adsorbate, leading to the work function decrease.

Because of the different mechanisms behind the work function decrease upon the AM and halides adsorption, changes in the work function with the coverage are significantly steeper when AM adatoms interact with platinum, while the effect of halides is more monotonous.

Upon concurrent presence of both AM and halides on the surface, it can be surmised, that co-adsorbed AM and halides adatoms would form ionic surface pairs that might neutralize each other's local field effect, possibly leading to reduced net dipole per adsorbed pair. Because of this, the work function decrease still will be seen, however, the Φ vs. coverage curve can demonstrate a nonmonotonic behavior depending on the alkali/halide ratio. Also, based on the dipole moment dependency on the coverage, it is conceivable that at low coverages alkali metal-induced Φ lowering may be a dominant, and shifting to intermediate and higher coverages halide adsorption could moderate the Φ drop.

This complex interplay of AM- and halide-induced changes in fundamental properties of Pt(111) could affect its electrocatalytic activity toward reactions, such as hydrogen evolution reaction (HER), and CO_2 reduction reaction (CO_2RR) and even enable suppression or promotion of selected processes. Specifically, the work function lowering can

facilitate electron donation of the surface, and weaken H adsorption, favoring the desorption step. For the processes involving CO_2, as discussed above, the combined effect of the AM and halides present on the surface can improve electron transfer to the molecule, enhancing its activation and stabilize possible intermediates such as CO_2^-, *COOH, and *CO, potentially leading to lower overpotentials.

Also, on platinum HER and CO_2RR are competing processes, with HER often overshadowing CO_2RR. While AM significantly lower work function, promoting the HER, halides may partially suppress HER by blocking key proton-adsorbing sites. Therefore, by carefully tuning halide coverage it could be possible to tip the balance in favor of the CO_2RR under specific conditions.

These conclusions require further study and confirmation, moreover, they do not account for the presence of actual electrochemical environment, where the effect of concurrent presence of AM and halides in the system can be more complex. It can involve interfacial water reorientation, affect water structure rigidity and introduce hydrogen bonding competition, affecting catalytic processes as the result. However, the present study paves the road toward more complicated models closer to realistic systems.

4. Conclusions

A density functional theory study has been conducted addressing the interaction of early alkaline metals with the Pt(111) surface from 0.06 ML coverage up to coverages where these overlayers still maintain a planar structure. While experimental studies are available for Na/Pt and K/Pt, adsorption of lithium at higher coverages has not been studied in detail. Hence our systematic study provides important insights for the understanding of the AM/Pt systems.

Overall, the early AM demonstrate a rather similar behavior with respect to their interaction with Pt(111). The sub-surface adsorption of all considered AM is energetically less favorable than adsorption on the surface, evidencing that AM/Pt composite systems are formed through deposition on the surface.

The maximum coverages for 2D overlayers were estimated to be 0.81 ML, 0.63 ML and 0.50 ML for Li, Na and K, respectively. A thorough analysis of the adsorption energies and geometries for the AM/Pt systems has been performed, in particular by regarding the evolution of the work function and charge distribution as a function of the coverage. The obtained results were found to be in good agreement with those available in the literature, at the same time expanding the available knowledge and offering more fundamental insights into the AM–Pt interaction.

At the lowest considered coverage, all studied alkali metals acquire a positive net charge upon adsorption and interact strongly with the platinum surface. Their impact on the properties of the substrate has a very localized nature, affecting only Pt atoms in direct contact with the adsorbate. Nonetheless, the adsorption of even single AM atom significantly lowers the work function of Pt(111).

Despite of each AM having a specific maximum coverage in their flat overlayers, their geometries at each given coverage are very similar to each other. At half-monolayer coverage all adlayers adopt a substrate-induced symmetry, similar to hexagonal, which largely remains preserved at higher Θ_{AM}. Furthermore, for all studied alkali metals, the depolarization of the adlayer with growing coverage is observed. As a result, at lower coverages up to 0.25 ML the adatoms mainly interact with the substrate, and adsorption of the adlayers is the most stable compared to the systems with higher Θ_{AM}. After reaching 0.25 ML coverage, the adatom–adatom interaction gradually increases, while adatom–substrate interaction decreases. Because of the overall larger decrease in the adatom–substrate component compared to the increase in the adatom–adatom one, the overall stability of the adlayer gradually decreases with the growing Θ_{AM}.

The tendency of the AM adatoms to lower the work function seen at the lowest 0.06 ML coverage remains when more than one atom is present on the surface. However after reaching 0.25 ML coverage for Na and K and 0.44 ML for Li, the work function of AM/Pt systems starts to increase. Based on the calculated dipole moment and the net positive charges decreasing with each added atom, this could be a combined result of the adlayer depolarization and the back donation of charge from Pt to the AM adlayers.

The obtained results provide deeper insights into the direct AM-Pt interaction and addresses possible outcomes of concurrent presence of AM atoms and halides on platinum surface. The analysis of the factors behind the growth and structure of the AM overlayers on platinum derived from our calculations will contribute to a better understanding of AM/Pt composites and of adlayer–substrate metallic systems in general.

CRediT authorship contribution statement

Andrey A. Koverga: Writing – original draft, Methodology, Investigation, Conceptualization. **Edson A. Ticianelli:** Writing – review & editing, Validation, Project administration, Methodology. **Axel Groß:** Writing – review & editing, Supervision, Software, Project administration, Methodology, Conceptualization.

Declaration of competing interest

The authors declare the following financial interests/personal relationships which may be considered as potential competing interests: Andrey A. Koverga reports financial support was provided by State of São Paulo Research Foundation. If there are other authors, they declare that they have no known competing financial interests or personal relationships that could have appeared to influence the work reported in this paper.

Acknowledgments

The authors would like to thank Fundação de Amparo a Pesquisa do Estado de São Paulo (FAPESP – Procs. 2022/13658-3), Brazil, for financial support and the federal state of Baden Württemberg through the bwHPC initiative together with the German Science Foundation (DFG) under grant no INST40/575-1 FUGG (JUSTUS 2 cluster) for providing the computational resources for the research.

Appendix A. Supplementary data

Supplementary material related to this article can be found online at https://doi.org/10.1016/j.apsusc.2025.164918.

Data availability

Data will be made available on request.

References

[1] M.C.O. Monteiro, F. Dattila, B. Hagedoorn, R. García-Muelas, N. López, M.T.M. Koper, Nat. Catal. 4 (2021) 654–662.
[2] A. Groß, Curr. Opin. Electrochem. 40 (2023) 101345.
[3] W. Schmickler, E. Santos, Interfacial Electrochemistry, second ed., Springer, Berlin, 2010.
[4] F. Gossenberger, T. Roman, A. Groß, Surf. Sci. 631 (2015) 17–22.
[5] F. Gossenberger, T. Roman, A. Groß, Electrochim. Acta 216 (2016) 152–159.
[6] J. Resasco, L.D. Chen, E. Clark, C. Tsai, C. Hahn, T.F. Jaramillo, K. Chan, A.T. Bell, J. Am. Chem. Soc. 139 (2017) 11277–11287.
[7] S. Ringe, E.L. Clark, J. Resasco, A. Walton, B. Seger, A.T. Bell, K. Chan, Energy Environ. Sci. 12 (2019) 3001–3014.
[8] A.S. Malkani, J. Anibal, B. Xu, ACS Catal. 10 (2020) 14871–14876.
[9] J. Tymoczko, V. Colic, A. Ganassin, W. Schuhmann, A.S. Bandarenka, Catal. Today 244 (2015) 96–102.
[10] S. Zhu, X. Hu, L. Zhang, M. Shao, J. Phys. Chem. C 120 (2016) 27452–27461.
[11] A.H. Shah, Z. Zhang, Z. Huang, S. Wang, G. Zhong, C. Wan, A.N. Alexandrova, Y. Huang, X. Duan, Nat. Catal. 5 (2022) 923–933.

[12] X. Li, G. Yang, Q. Zhang, Z. Liu, F. Peng, J. Phys. Chem. Lett. 14 (2023) 11177–11182.
[13] C.A. Angelucci, H. Varela, G. Tremiliosi-Filho, J.F. Gomes, Electrochem. Commun. 33 (2013) 10–13.
[14] G. Ertl, Catal. Rev. 21 (1980) 201–223.
[15] A. Borodziński, G.C. Bond, Catal. Rev. 50 (2008) 379–469.
[16] G.A. Somorjai, F. Zaera, J. Phys. Chem. 86 (1982) 3070–3078.
[17] J. Crowell, E. Garfunkel, G. Somorjai, Surf. Sci. 121 (1982) 303–320.
[18] M. Kiskinova, G. Pirug, H. Bonzel, Surf. Sci. 133 (1983) 321–343.
[19] Z. Liu, Y. Zhou, F. Solymosi, J. White, Surf. Sci. 245 (3) (1991) 289–304.
[20] A.P. Farkas, F. Solymosi, J. Phys. Chem. C 113 (2009) 19930–19936.
[21] W. Liao, P. Liu, ACS Catal. 10 (2020) 5723–5733.
[22] J. Li, X. Li, C.M. Gunathunge, M.M. Waegele, Proc. Natl. Acad. Sci. 116 (2019) 9220–9229.
[23] D. Le, T.S. Rahman, Nat. Catal. 5 (2022) 977–978.
[24] M. Watanabe, M. Horiuchi, S. Motoo, J. Electroanal. Chem. Interfacial Electrochem. 250 (1988) 117–125.
[25] S.A. Campbell, R. Parsons, J. Chem. Soc. Faraday Trans. 88 (1992) 833.
[26] A. Groß, J. Comput. Theor. Nanosci. 5 (2008) 894.
[27] Y. Kwon, T.J.P. Hersbach, M.T.M. Koper, Top. Catal. 57 (2014) 1272–1276.
[28] M.C. Figueiredo, O. Sorsa, N. Doan, E. Pohjalainen, H. Hildebrand, P. Schmuki, B.P. Wilson, T. Kallio, J. Power Sources 275 (2015) 341–350.
[29] G.L. Caneppele, T.S. Almeida, C.R. Zanata, É. Teixeira-Neto, P.S. Fernández, G.A. Camara, C.A. Martins, Appl. Catal. B: Environ. 200 (2017) 114–120.
[30] A. Boronat-González, E. Herrero, J.M. Feliu, Curr. Opin. Electrochem. 4 (2017) 26–31.
[31] A. Koverga, E. Flórez, M.A. Gómez-Marín, Appl. Surf. Sci. 608 (2023) 155137.
[32] N. Furuya, S. Motoo, J. Electroanal. Chem. Interfacial Electrochem. 78 (1977) 243–256.
[33] M.T. Paffett, C.T. Campbell, T.N. Taylor, J. Chem. Phys. 85 (1986) 6176–6185.
[34] I.A. Pašti, N.M. Gavrilov, S.V. Mentus, Adv. Phys. Chem. 1 (2011) 1–8.
[35] I. Pašti, S. Mentus, 11 (2009) 6225.
[36] J.V. Perales-Rondón, J. Solla-Gullón, E. Herrero, C.M. Sánchez-Sánchez, Appl. Catal. B: Environ. 201 (2017) 48–57.
[37] H.-X. Liu, N. Tian, M.P. Brandon, Z.-Y. Zhou, J.-L. Lin, C. Hardacre, W.-F. Lin, S.-G. Sun, ACS Catal. 2 (2012) 708–715.
[38] H.-X. Liu, N. Tian, M.P. Brandon, J. Pei, Z.-C. Huangfu, C. Zhan, Z.-Y. Zhou, C. Hardacre, W.-F. Lin, S.-G. Sun, Phys. Chem. Chem. Phys. 14 (2012) 16415.
[39] Q.-S. Chen, Z.-Y. Zhou, F.J. Vidal-Iglesias, J. Solla-Gullon, J.M. Feliu, S.-G. Sun, J. Am. Chem. Soc. 133 (2011) 12930–12933.
[40] I. Ledezma-Yanez, W.D.Z. Wallace, P. Sebastián-Pascual, V. Climent, J.M. Feliu, M.T.M. Koper, Nat. Energy 2 (2017) 1–7.
[41] F.J. Sarabia, V. Climent, J.M. Feliu, 20 (2019) 3056–3066.
[42] I.T. McCrum, M.T.M. Koper, Nat. Energy 5 (2020) 891–899.
[43] T. Aruga, Prog. Surf. Sci. 31 (1989) 61–130.
[44] H. Bonzel, Surf. Sci. Rep. 8 (1988) 43–125.
[45] J. Lehmann, P. Roos, E. Bertel, Phys. Rev. B 54 (1996) R2347–R2350.
[46] S. Moré, W. Berndt, A.M. Bradshaw, R. Stumpf, Phys. Rev. B 57 (1998) 9246–9254.
[47] S. Moré, A.P. Seitsonen, W. Berndt, A.M. Bradshaw, Phys. Rev. B 63 (2001) 075406.
[48] I.T. Roe, S.K. Schnell, J. Mater. Chem. A 9 (2021) 11042–11048.
[49] G. Kresse, J. Hafner, Phys. Rev. B 47 (1993) 558–561.
[50] G. Kresse, J. Hafner, Phys. Rev. B 49 (1994) 14251–14269.
[51] G. Kresse, J. Furthmuller, Phys. Rev. B 54 (1996) 11169–11186.
[52] G. Kresse, Furthmuller, Comput. Mater. Sci. 6 (1996) 15–50.
[53] J.P. Perdew, K. Burke, M. Ernzerhof, Phys. Rev. Lett. 77 (18) (1996) 3865–3868.
[54] F. Gossenberger, T. Roman, K. Forster-Tonigold, A. Groß, Beilstein J. Nanotechnol. 5 (2014) 152–161.
[55] D.D.V. Anićijević, V.M. Nikolić, M.P. Marčeta-Kaninski, I.A. Pašti, Int. J. Hydrog. Energy 38 (2013) 16071–16079.
[56] M.J. Ungerer, D. Santos-Carballal, A. Cadi-Essadek, C.G.C.E. van Sittert, N.H. de Leeuw, J. Phys. Chem. C 123 (2019) 27465–27476.
[57] K. Okuda, M. Alaydrus, N. Hoshi, I. Hamada, M. Nakamura, J. Phys. Chem. C 126 (2022) 4726–4732.
[58] P.E. Blöchl, Phys. Rev. B 50 (1994) 17953–17979.
[59] G. Kresse, D. Joubert, Phys. Rev. B 59 (1999) 1758–1775.
[60] H.J. Monkhorst, J.D. Pack, Phys. Rev. B 13 (1976) 5188–5192.
[61] M. Methfessel, A.T. Paxton, Phys. Rev. B 40 (1989) 3616–3621.
[62] I. Pašti, S. Mentus, J. Alloys Compd. 497 (2010) 38–45.
[63] K. Reuter, M. Scheffler, Phys. Rev. B 65 (2001) 035406.
[64] K. Sarkar, D. Hübner, D. Stottmeister, A. Groß, Phys. Rev. Mater. 8 (2024) 015401.
[65] M. Mavrikakis, B. Hammer, J.K. Nørskov, Phys. Rev. Lett. 81 (1998) 2819.
[66] R.J. Behm, A. Groß, Surf. Sci. 754 (2025) 122677.
[67] A.A. Koverga, E. Flórez, C. Jimenez-Orozco, J.A. Rodriguez, Electrochim. Acta 368 (2021) 137598.
[68] T.A. Manz, D.S. Sholl, J. Chem. Theory Comput. 8 (2012) 2844–2867.
[69] T.A. Manz, N.G. Limas, RSC Adv. 6 (2016) 47771–47801.
[70] N.G. Limas, T.A. Manz, RSC Adv. 6 (2016) 45727–45747.
[71] A.A. Koverga, S. Frank, M.T. Koper, Electrochim. Acta 101 (2013) 244–253.
[72] F. Saad, M. Zemirli, M. Benakki, S. Bouarab, Phys. B 407 (2012) 698–704.
[73] I. Matanovic, P. Atanassov, F. Garzon, N.J. Henson, ECS Trans. 61 (2014) 47–53.
[74] J.N. Mills, I.T. McCrum, M.J. Janik, Phys. Chem. Chem. Phys. 16 (2014) 13699–13707.
[75] L. Pauling, J. Am. Chem. Soc. 69 (1947) 542–553.
[76] M. Sotoudeh, S. Baumgart, M. Dillenz, J. Döhn, K. Forster-Tonigold, K. Helmbrecht, D. Stottmeister, A. Groß, Adv. Energy Mater. 14 (2024) 2302550.
[77] F.L. Hirshfeld, Theor. Chim. Acta 44 (1977) 129–138.
[78] R.F.W. Bader, Atoms in Molecules: A Quantum theory, Oxford University Press, Oxford, U.K., 1990.
[79] A.V. Marenich, S.V. Jerome, C.J. Cramer, D.G. Truhlar, J. Chem. Theory Comput. 8 (2012) 527–541.
[80] R.S. Mulliken, J. Chem. Phys. 23 (1955) 1833–1840.
[81] B.H. Besler, K.M. Merz, P.A. Kollman, J. Comput. Chem. 11 (1990) 431–439.
[82] A.E. Reed, R.B. Weinstock, F. Weinhold, J. Chem. Phys. 83 (1985) 735–746.
[83] C. Campañá, B. Mussard, T.K. Woo, J. Chem. Theory Comput. 5 (2009) 2866–2878.
[84] A. Allred, J. Inorg. Nucl. Chem. 17 (1961) 215–221.
[85] P. Polestshuk, Nat. Commun. 15 (2024) 10404.
[86] S. Trasatti, J. Electroanal. Chem. Interfacial Electrochem. 39 (1972) 163–184.
[87] S. Sarkar, S.D. Ramarao, T. Das, R. Das, C.P. Vinod, S. Chakraborty, S.C. Peter, ACS Catal. 11 (2021) 800–808.
[88] A.A. Koverga, A.M. Gómez-Marín, E. Flórez, J. Phys. Chem. C 126 (2022) 10167–10180.
[89] H.P. Bonzel, G. Pirug, C. Ritke, Langmuir 7 (1991) 3006–3011.
[90] H. Bonzel, G. Pirug, A. Winkler, Chem. Phys. Lett. 116 (1985) 133–137.
[91] D.L. Doering, S. Semancik, T.E. Madey, Surf. Sci. 133 (1983) 49–70.
[92] S.-A. Lindgren, J. Paul, L. Walldén, Surf. Sci. 155 (1985) 165–172.
[93] R. Gerlach, T. Rhodin, Surf. Sci. 19 (1970) 403–426.
[94] S. Trasatti, Comprehensive Treatise of Electrochemistry, Springer US, 1980, pp. 45–81.
[95] Y.-X. Wang, G.-C. Wang, ACS Catal. 9 (2019) 2261–2274.
[96] Y.-P. Ma, G.-C. Wang, J. Phys. Chem. C 127 (2022) 265–278.
[97] B.A. Rohr, A.R. Singh, J.K. Nørskov, J. Catalysis 372 (2019) 33–38.
[98] L. Zhang, J. Han, H. Wang, R. Car, W. E, Phys. Rev. Lett. 120 (2018) 143001.